



Figures and figure supplements

Inactivation of the ATMIN/ATM pathway protects against glioblastoma formation

Sophia M Blake et al

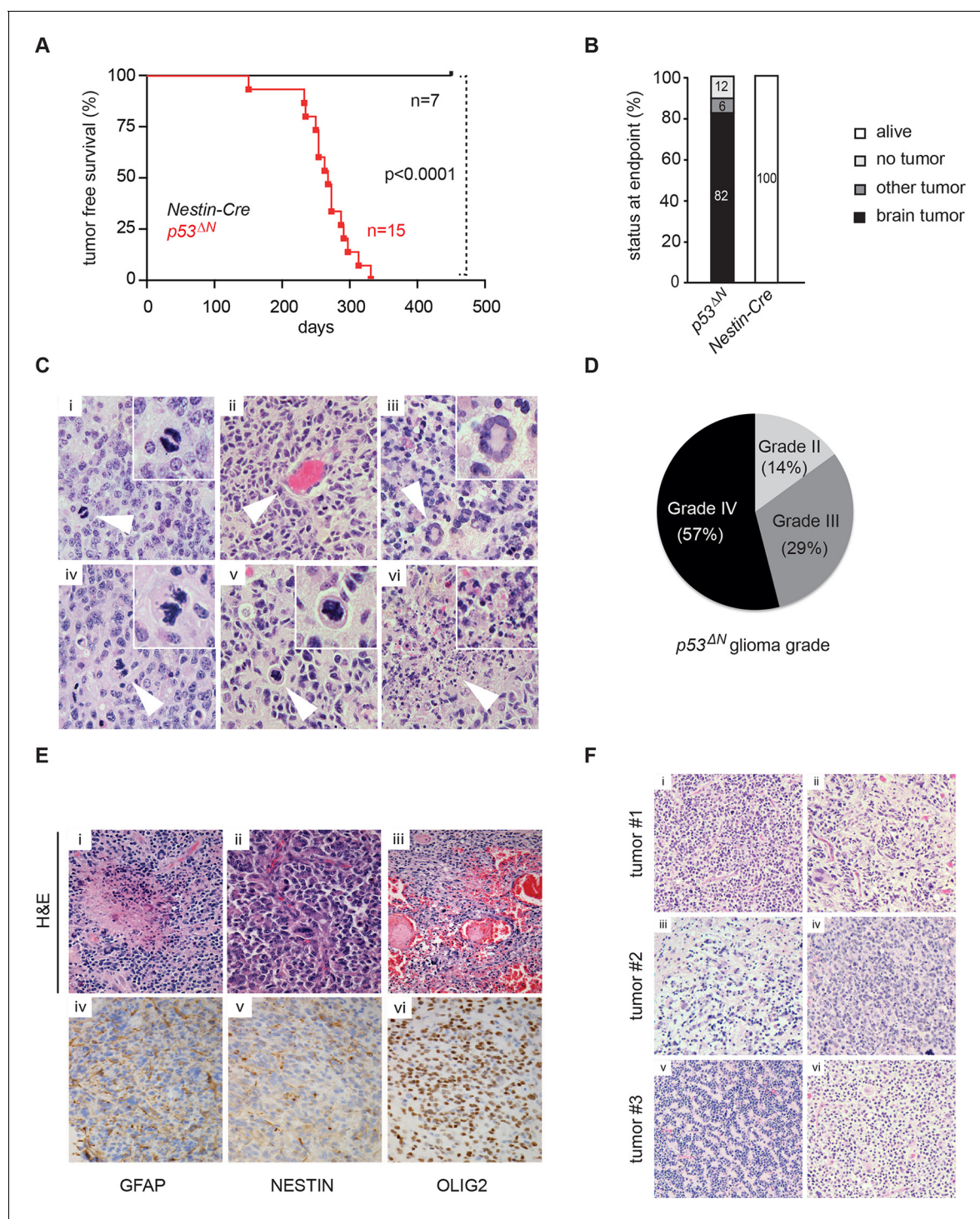


Figure 1. Loss of *Trp53* is sufficient to induce GBM with high penetrance. (A) Kaplan-Meier curves showing tumor-free survival in *p53^{fl/fl}; Nestin-Cre* (*p53^{AN}*) and control *Nestin-Cre* mice. (B) Status of mouse cohorts at 450 days, showing tumor incidence. (C) H&E-stained *p53^{AN}* brain tumor sections showing histological features of malignant GBM. Arrowheads indicate (i) a mitotic cell, (ii) neo-vascularization, (iii) rosetta formation, (iv) mitotic catastrophe, (v) a multinucleated giant cell, and (vi) large areas of necrosis. (D) Grades of gliomas for *p53^{AN}* mice. (E) Examples of human GBM hallmarks observed in *p53^{AN}* tumors: pseudopalisading necrosis (i), microvascular proliferation with endothelial hyperplasia (ii), and endovascular thrombosis (iii) (all H&E). Immunohistochemistry shows expression of the glial markers GFAP (iv), NESTIN (v), and OLIG2 (vi) in *p53^{AN}* tumors. (F) *p53^{AN}* glioblastomas display high inter- and intra-tumoral heterogeneity. H&E images i-ii, iii-iv, and v-vi represent different regions of the same tumors #1, #2, and #3 respectively. GBM, Glioblastoma multiforme.

DOI: 10.7554/eLife.08711.003

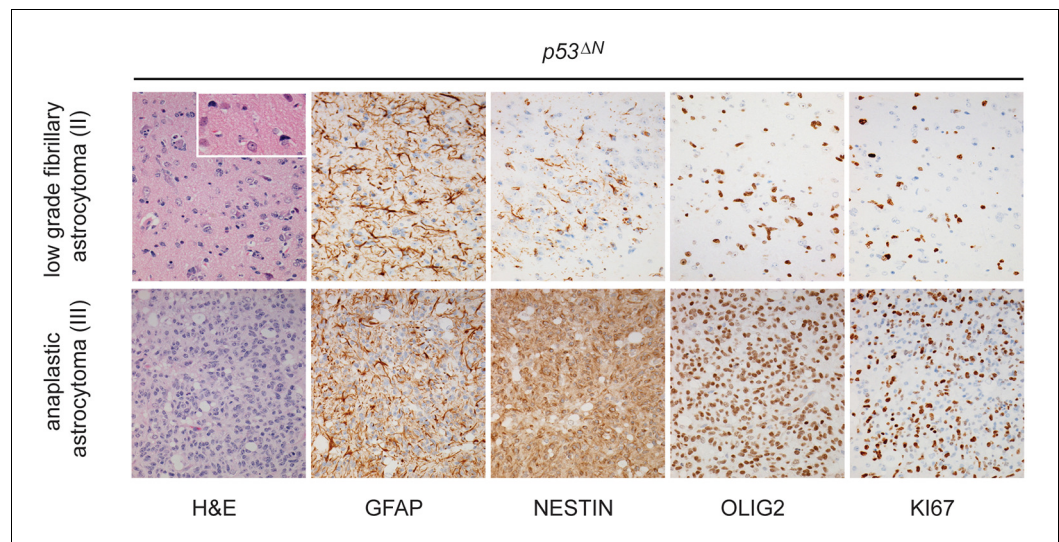


Figure 1—figure supplement 1. Histological features of lower grade tumors observed in $p53^{\Delta N}$ animals. Hematoxylin and Eosin (H&E) and antibody-stained sections of $p53^{\Delta N}$ brains showing representative examples of low-grade fibrillary astrocytoma (WHO Grade II) and anaplastic astrocytoma (WHO Grade III). Ki67 immunolabeling indicates progressively increased proliferation of atypical glial cells with increased tumor grade
DOI: [10.7554/eLife.08711.004](https://doi.org/10.7554/eLife.08711.004)

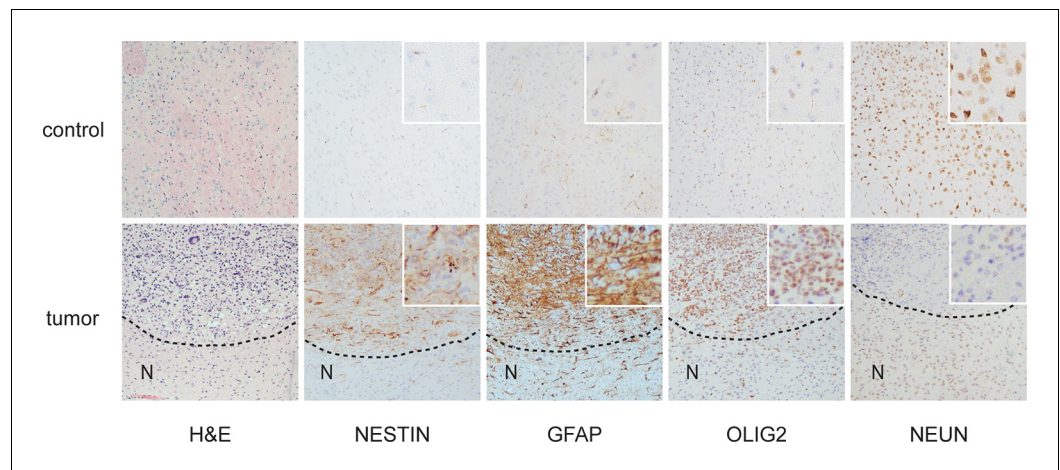


Figure 1—figure supplement 2. Histological features of glioblastomas observed in $p53^{\Delta N}$ animals. H&E and immunohistochemical staining of sections from $p53^{\Delta N}$ control brain tissue (top row) and gliomas (lower row). 'N' denotes the normal brain region adjacent to the tumor mass.
[DOI: 10.7554/eLife.08711.005](https://doi.org/10.7554/eLife.08711.005)

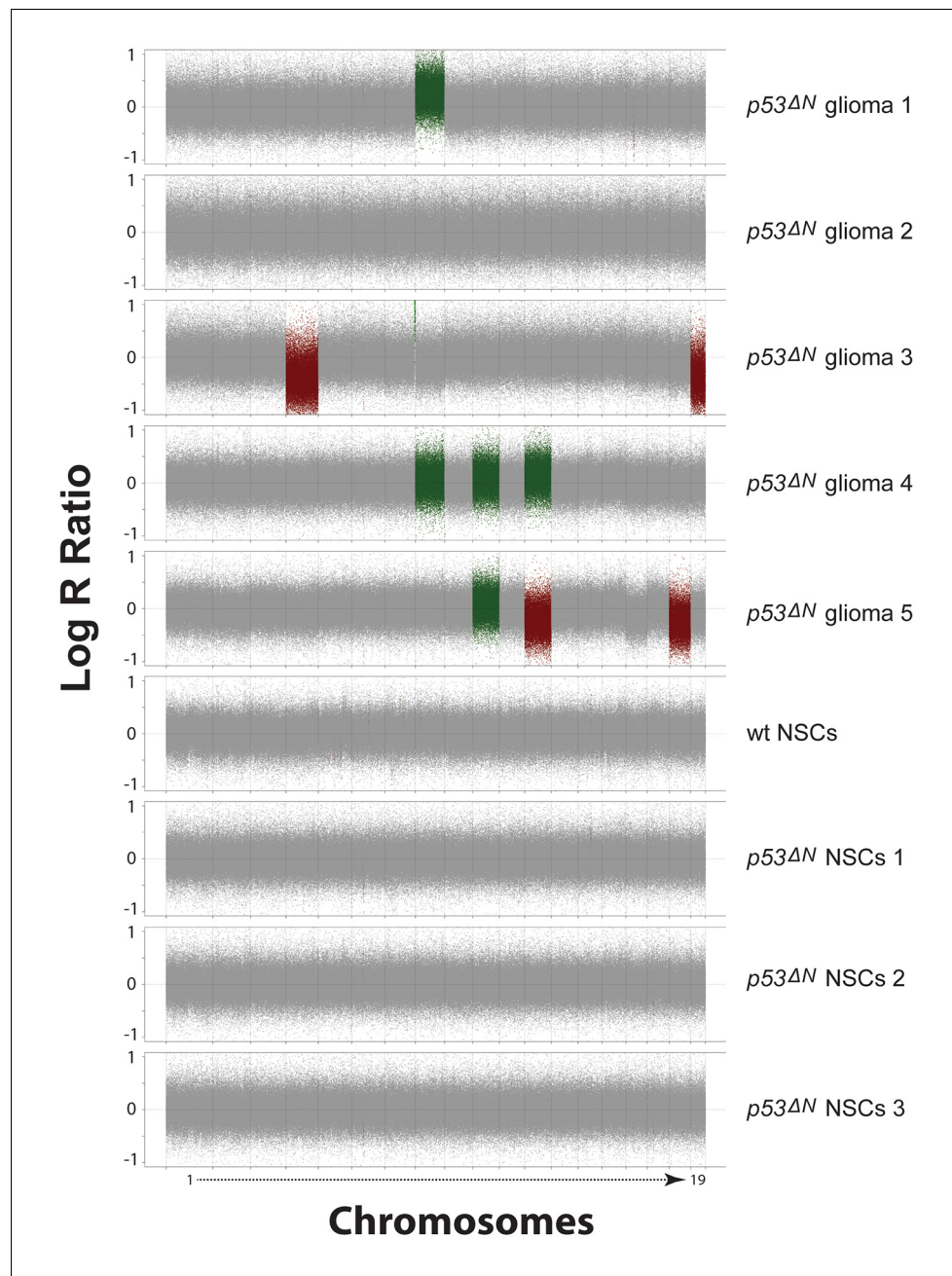


Figure 1—figure supplement 3. SNP array analysis on primary cells derived from GBM bearing $p53^{\Delta N}$, non-tumor bearing $p53^{\Delta N}$, and wild-type (wt) animals. Chromosomal copy number variations are found in primary tumor cells derived from $p53^{\Delta N}$ gliomas (Stupp et al., 2005; Wen and Kesari, 2008; Cancer Genome Atlas Research Network, 2008; Wen et al., 2006; Rich et al., 2004) but not in non-tumorous adult $p53^{\Delta N}$ NSCs (Stupp et al., 2005; Wen and Kesari, 2008; Cancer Genome Atlas Research Network, 2008) or adult wt NSCs. Log R Ratio plots show copy number states for all mouse autosomes for tumor, wt, and $p53^{\Delta N}$ cells. Grey points represent probes in a normal copy number state. Green and light green represents gain and amplification calls, respectively, while red and light red points represent hemi- and homozygous losses, respectively. NSC, Neural stem cell.
DOI: [10.7554/eLife.08711.006](https://doi.org/10.7554/eLife.08711.006)

Chr	Start	End	p53ΔN glioma 1	p53ΔN glioma 2	p53ΔN glioma 3	p53ΔN glioma 4	p53ΔN glioma 5	wt NSCs	p53ΔN NSCs 1	p53ΔN NSCs 2	p53ΔN NSCs 3	Larger_than_1000Kb
1	3036178	155529710	2	2	2	2	2	2	2	2	2	TRUE
1	155537885	172174846	2	2	2	2	2	2	2	2	2	TRUE
1	172175790	176957404	2	2	2	2	2	2	2	2	2	TRUE
1	176979749	191080460	2	2	2	2	2	2	2	2	2	TRUE
1	191185601	197191885	2	2	2	2	2	2	2	2	2	TRUE
2	3011992	23617630	2	2	2	2	2	2	2	2	2	TRUE
2	23689775	120285803	2	2	2	2	2	2	2	2	2	TRUE
2	120292119	181731081	2	2	2	2	2	2	2	2	2	TRUE
3	3033414	52327081	2	2	2	2	2	2	2	2	2	TRUE
3	52329358	159598996	2	2	2	2	2	2	2	2	2	TRUE
4	3136962	72564529	2	2	1	2	2	2	2	2	2	TRUE
4	72630403	90574624	2	2	1	2	2	2	2	2	2	TRUE
4	90575886	155559551	2	2	1	2	2	2	2	2	2	TRUE
5	3075868	76268752	2	2	2	2	2	2	2	2	2	TRUE
5	76300210	109050082	2	2	2	2	2	2	2	2	2	TRUE
5	109153628	149576175	2	2	2	2	2	2	2	2	2	TRUE
5	149609250	152527863	2	2	2	2	2	2	2	2	2	TRUE
6	3150188	20453205	2	2	2	2	2	2	2	2	2	TRUE
6	20460309	47593502	2	2	2	2	2	2	2	2	2	TRUE
6	47730360	57624236	2	2	2	2	2	2	2	2	2	TRUE
6	57826208	60647058	2	2	2	2	2	2	2	2	2	TRUE
6	60991556	83759424	2	2	2	2	2	2	2	2	2	TRUE
6	83969109	149505351	2	2	2	2	2	2	2	2	2	TRUE
7	3123840	54656603	2	2	2	2	2	2	2	2	2	TRUE
7	54976185	93054737	2	2	2	2	2	2	2	2	2	TRUE
7	93148417	104419396	2	2	2	2	2	2	2	2	2	TRUE
7	104560225	148352711	2	2	2	2	2	2	2	2	2	TRUE
7	149619422	152084142	2	2	4	2	2	2	2	2	2	TRUE
8	3090670	7508707	3	2	2	3	2	2	2	2	2	TRUE
8	7512937	28527069	3	2	2	3	2	2	2	2	2	TRUE
8	28707166	112671618	3	2	2	3	2	2	2	2	2	TRUE
8	112681177	131706890	3	2	2	3	2	2	2	2	2	TRUE
9	3097506	5674350	2	2	2	2	2	2	2	2	2	TRUE
9	5688507	124029861	2	2	2	2	2	2	2	2	2	TRUE
10	3009281	127599933	2	2	2	3	3	2	2	2	2	TRUE
10	127627785	12982856	2	2	2	3	3	2	2	2	2	TRUE
11	3011548	102477094	2	2	2	2	2	2	2	2	2	TRUE
11	102481278	121829163	2	2	2	2	2	2	2	2	2	TRUE
12	3136333	55195889	2	2	2	3	1	2	2	2	2	TRUE
12	55199385	121256667	2	2	2	3	1	2	2	2	2	TRUE
13	3011215	11969361	2	2	2	2	2	2	2	2	2	TRUE
13	12139804	65318306	2	2	2	2	2	2	2	2	2	TRUE
13	65344931	74877016	2	2	2	2	2	2	2	2	2	TRUE
13	74882325	117492948	2	2	2	2	2	2	2	2	2	TRUE
13	117501690	120259651	2	2	2	2	2	2	2	2	2	TRUE
14	7761318	12673699	2	2	2	2	2	2	2	2	2	TRUE
14	12677416	69888463	2	2	2	2	2	2	2	2	2	TRUE
14	70098891	125118724	2	2	2	2	2	2	2	2	2	TRUE
15	3096128	103458457	2	2	2	2	2	2	2	2	2	TRUE
16	3284445	35466618	2	2	2	2	2	2	2	2	2	TRUE
16	35597168	40755838	2	2	2	2	2	2	2	2	2	TRUE
16	41384667	98290818	2	2	2	2	2	2	2	2	2	TRUE
17	3087345	30602119	2	2	2	2	2	2	2	2	2	TRUE
17	30809092	79700136	2	2	2	2	2	2	2	2	2	TRUE
17	79704238	95264893	2	2	2	2	2	2	2	2	2	TRUE
18	3149782	90766409	2	2	2	2	1	2	2	2	2	TRUE
19	3159638	61337203	2	2	1	2	2	2	2	2	2	TRUE

Figure 1—figure supplement 4. Table representing CGHcall output for SNP array analysis compressed to comparable regions between arrays in the series. Genomic position and corresponding CGHcall copy number state of samples (0 – homozygous loss, 1 – hemizygous loss, 2 – normal state, 3 – gain, 4 – amplification) are included in the table.

DOI: 10.7554/eLife.08711.007

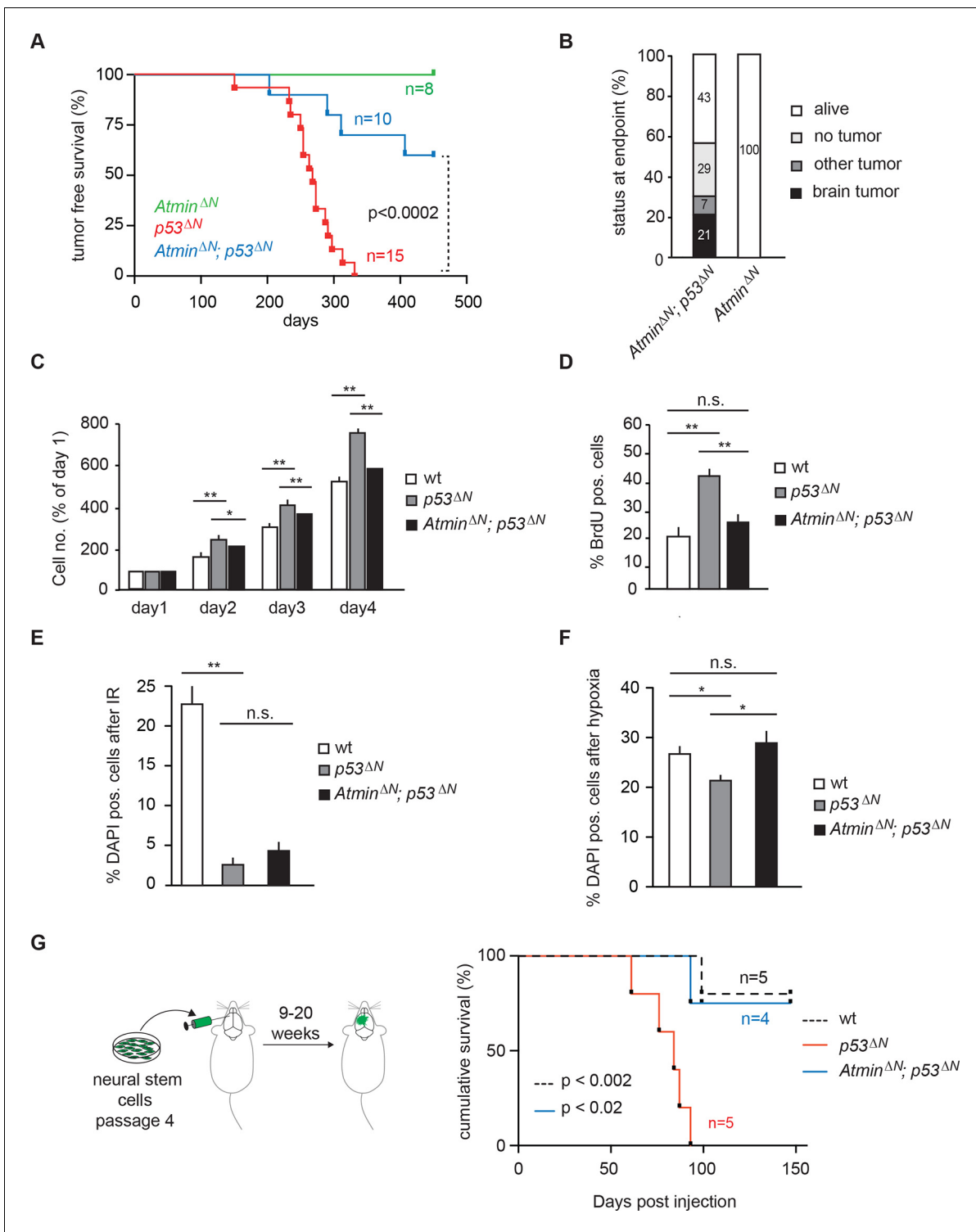


Figure 2. Loss of *Atmin* rescues GBM formation in *p53*^{ΔN} brains. (A) Kaplan-Meier curves showing tumor-free survival in *Atmin*^{ΔN} and *Atmin*^{ΔN}; *p53*^{ΔN} mice. *p53*^{ΔN} curve from **Figure 1A** (same experiment) is shown for comparison. (B) Status of mouse cohorts at 450 days, showing tumor incidence. (C) *Atmin* loss rescues the increased proliferation of *p53*^{ΔN} NSCs. (D) Mean percentage of BrdU-positive NSCs from the indicated genotypes, assessed by FACS following a 2-hr BrdU pulse. (E) Mean number of DAPI-permeable (non-viable) cells after IR or (F) hypoxia, showing sensitivity of *Atmin*^{ΔN}; *p53*^{ΔN} NSCs to hypoxia but not IR. n.s., not significant; * *p* < 0.05, ** *p* < 0.01. (G) Scheme of orthotopic NSC transplant experiment (left) and Kaplan-Meier curves indicating survival of NOD/SCID mice orthotopically transplanted with *p53*^{ΔN} and *Atmin*^{ΔN}; *p53*^{ΔN} NSCs (right). Error bars represent the SEM of three biological repeats, and two biological repeats for (E). IR, Ionizing radiation; NSC, Neural stem cell.

Figure 2 continued on next page

Figure 2 continued

DOI: [10.7554/eLife.08711.008](https://doi.org/10.7554/eLife.08711.008)

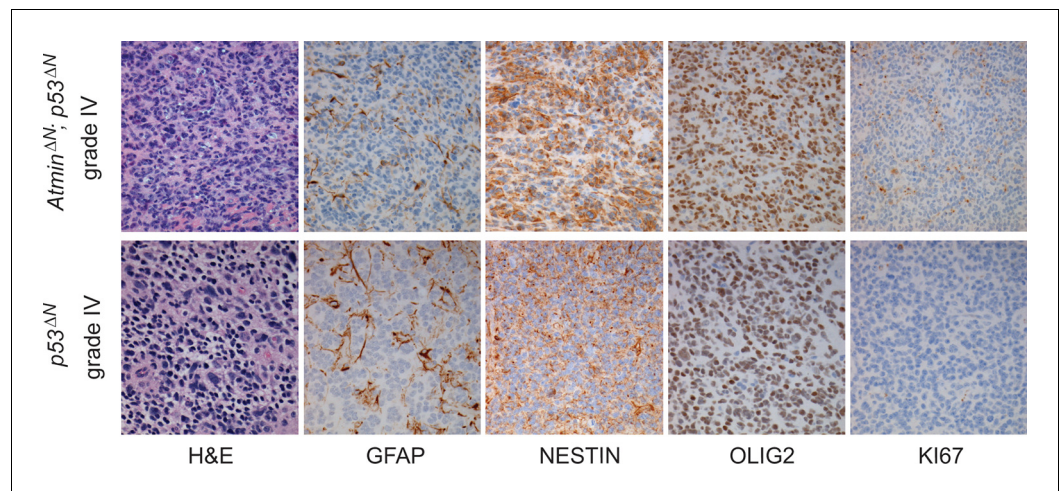


Figure 2—figure supplement 1. Histological features of glioblastomas observed in $p53^{\Delta N}$ and $Atmin^{\Delta N}; p53^{\Delta N}$ animals. H&E and immunohistochemical staining of sections from gliomas derived from $Atmin^{\Delta N}; p53^{\Delta N}$ brains (top row) showing expression of Nestin and Olig2 in the tumor cells as well as scattered expression of Gfap, similar to Grade IV GBMs from $p53^{\Delta N}$ animals (lower row).

DOI: [10.7554/eLife.08711.009](https://doi.org/10.7554/eLife.08711.009)

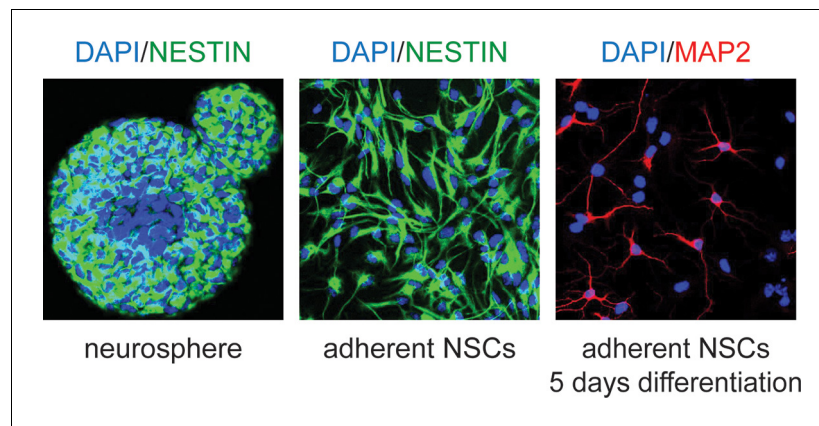


Figure 2—figure supplement 2. Examples of murine neural stem cells in culture. Neural stem cells (NSCs) were isolated according to published protocols and cultured first as neurospheres (left), then maintained in adherent culture (center). They maintain the ability to differentiate, as shown by Map2 staining after 5 days (right).

DOI: [10.7554/eLife.08711.010](https://doi.org/10.7554/eLife.08711.010)

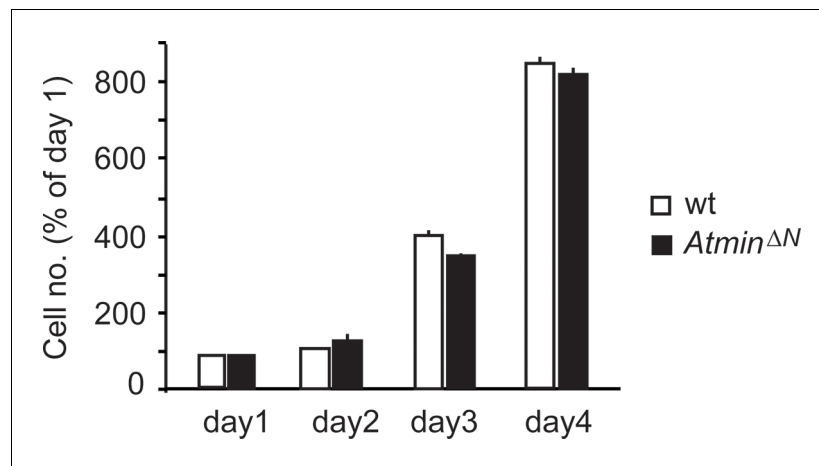


Figure 2—figure supplement 3. *Atmin*^{ΔN} NSCs proliferate at a similar rate as wild-type NSCs. Error bars represent the SEM of two biological repeats. NSC, Neural stem cell.

DOI: [10.7554/eLife.08711.011](https://doi.org/10.7554/eLife.08711.011)

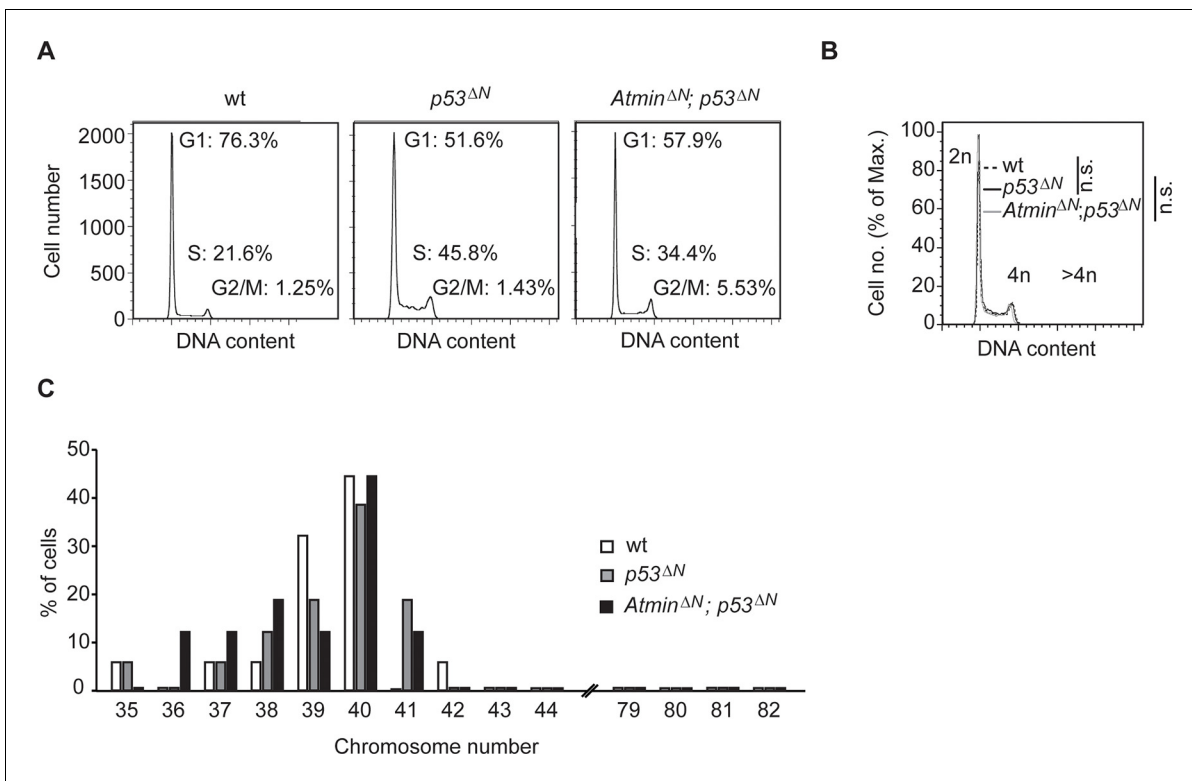


Figure 2—figure supplement 4. Gross genome stability is unaffected in *Atmin/Trp53* double mutant NSCs. (A) Percentages of cells in G1, S and G2/M cell cycle phases, as measured by FACS. (B) *Atmin^{ΔN}; p53^{ΔN}* and *p53^{ΔN}* NSCs have similar proportions of cells with >4n DNA content as wild-type NSCs, as judged by FACS of propidium iodide (PI)-stained cells. Representative images of two biological repeats per genotype are shown for (A) and (B). (C) Metaphase spread analysis of chromosome number from NSCs of the indicated genotypes. At least 15 cells were analyzed for each indicated genotype. NSC, Neural stem cell.

DOI: 10.7554/eLife.08711.012

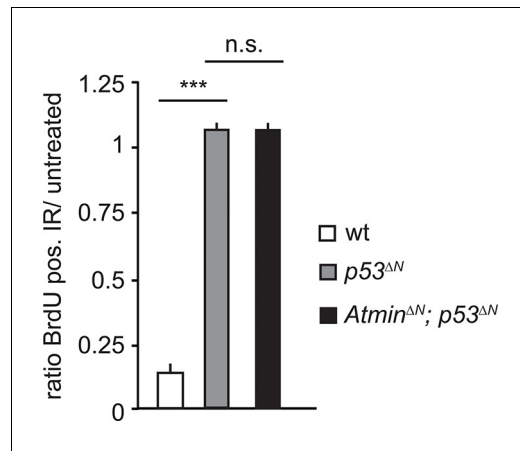


Figure 2—figure supplement 5. Radiation-induced arrest is similarly impaired in *Trp53*-mutant and *Atmin/Trp53* double mutant NSCs. Mean average ratio of BrdU-positive IR-treated NSCs relative to untreated NSCs, showing similar impaired arrest in *Atmin*^{ΔN}; *p53*^{ΔN} and *p53*^{ΔN} NSCs. Error bars represent the SEM of two biological repeats. IR, Ionizing radiation; NSC, Neural stem cell.

DOI: [10.7554/eLife.08711.013](https://doi.org/10.7554/eLife.08711.013)

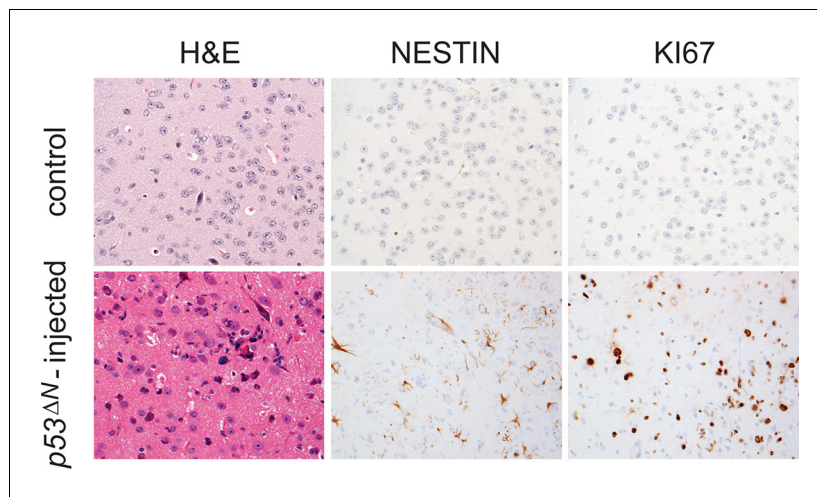


Figure 2—figure supplement 6. Tumors arising from orthotopic injection of NSCs are Nestin and Ki67-positive. Adjacent sections from a representative tumor arising from injected p53 Δ N NSCs stained with Nestin and Ki67. Control, uninjected brain. NSC, Neural stem cell.

DOI: [10.7554/eLife.08711.014](https://doi.org/10.7554/eLife.08711.014)

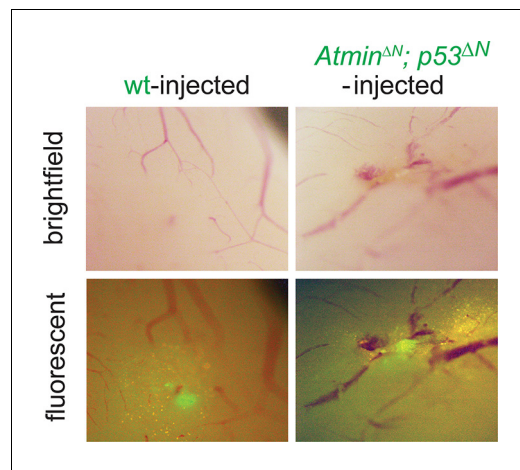


Figure 2—figure supplement 7. Asymptomatic *Atmin*^{ΔN}; *p53*^{ΔN}-injected animals show persistent GFP-positive cells. Bright field and fluorescent images of asymptomatic mouse brains 155 days after injection with wt or *Atmin*^{ΔN}; *p53*^{ΔN} NSCs, showing persistence of injected cells. NSC, Neural stem cell

DOI: [10.7554/eLife.08711.015](https://doi.org/10.7554/eLife.08711.015)

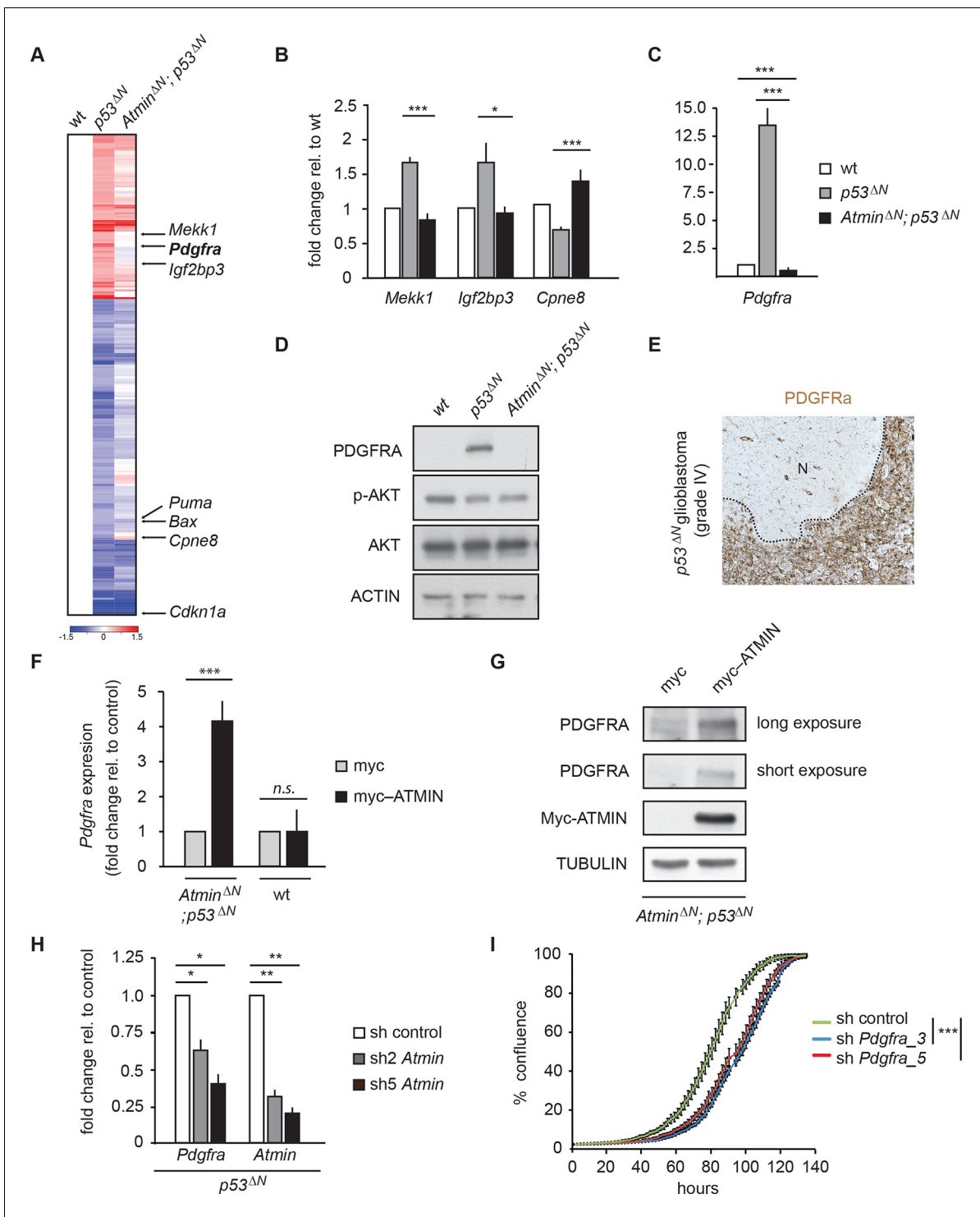


Figure 3. Atmin regulates *Pdgfra* expression in a mutant *Trp53* background. (A) Heatmap showing genes deregulated more than 1.5-fold in *Trp53* null NCS and their corresponding expression in *Atmin^{ΔN}; p53^{ΔN}* double null NCS. (B, C) qRT-PCR validation of GBM implicated genes that show deregulated expression in *p53^{ΔN}* but not *Atmin^{ΔN}; p53^{ΔN}* NCS. (D) Elevated *Pdgfra* protein expression in *p53^{ΔN}* but not *Atmin^{ΔN}; p53^{ΔN}* NCS. Corresponding p-Akt and total Akt levels were probed to analyze pathway activation. Actin was used as loading control. (E) Tumor section from a GBM arising from a *p53^{ΔN}* animal showing elevated *Pdgfra* expression. 'N' denotes the normal brain region adjacent to the tumor mass. Dotted lines indicate tumor border. (F) Myc-Atmin overexpression increases expression of *Pdgfra* mRNA in *Atmin^{ΔN}; p53^{ΔN}* but not wt cells. (G) Myc-Atmin overexpression increases *Pdgfra* protein levels in *Atmin^{ΔN}; p53^{ΔN}* NCS. Tubulin was used as loading control. (H) *Atmin* silencing using two independent shRNA constructs reduces *Pdgfra* expression, assessed by qRT-PCR. (I) Stable *Pdgfra* silencing using two independent shRNA constructs

Figure 3 continued on next page

Figure 3 continued

reduces primary tumor cell proliferation, measured using IncuCyte timelapse microscopy. Error bars represent the SEM of at least three biological repeats and two biological repeats in (I). * $p < 0.05$, ** $p < 0.01$, *** $p < 0.001$. NSC, Neural stem cell

DOI: [10.7554/eLife.08711.016](https://doi.org/10.7554/eLife.08711.016)

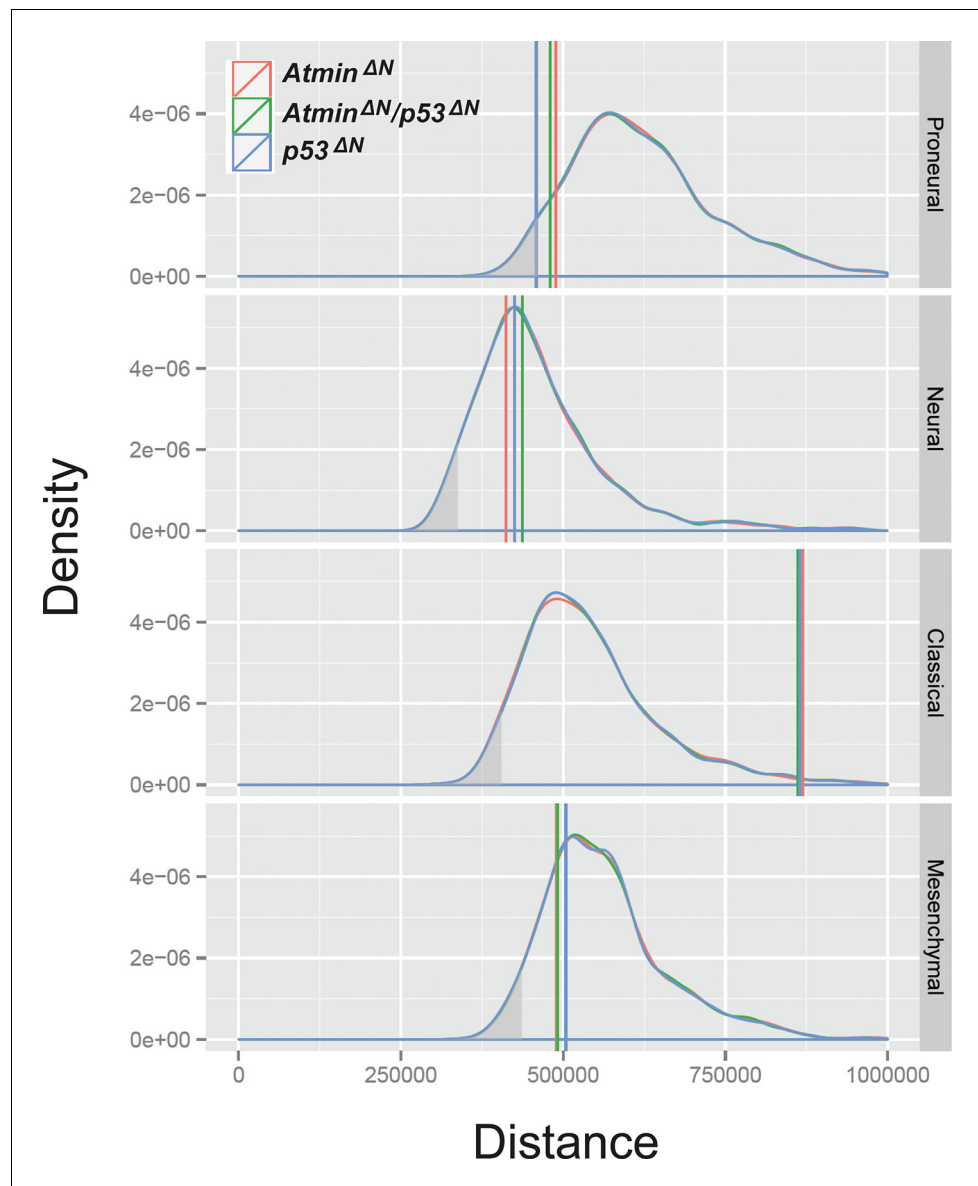


Figure 3—figure supplement 1. The transcriptional profile of *p53*^{ΔN} NSCs is most closely related to the human proneural GBM subtype, relative to expected distances. Relative to expected distance away from the centroids, *p53*^{ΔN} is closest to the proneural category ($p=0.036$, simulation test) and the *p53*^{ΔN}:proneural pairing is the only one that is significant – the grey shading represents the lower 5% tail of the simulated distances. NSC, Neural stem cell

DOI: [10.7554/eLife.08711.017](https://doi.org/10.7554/eLife.08711.017)

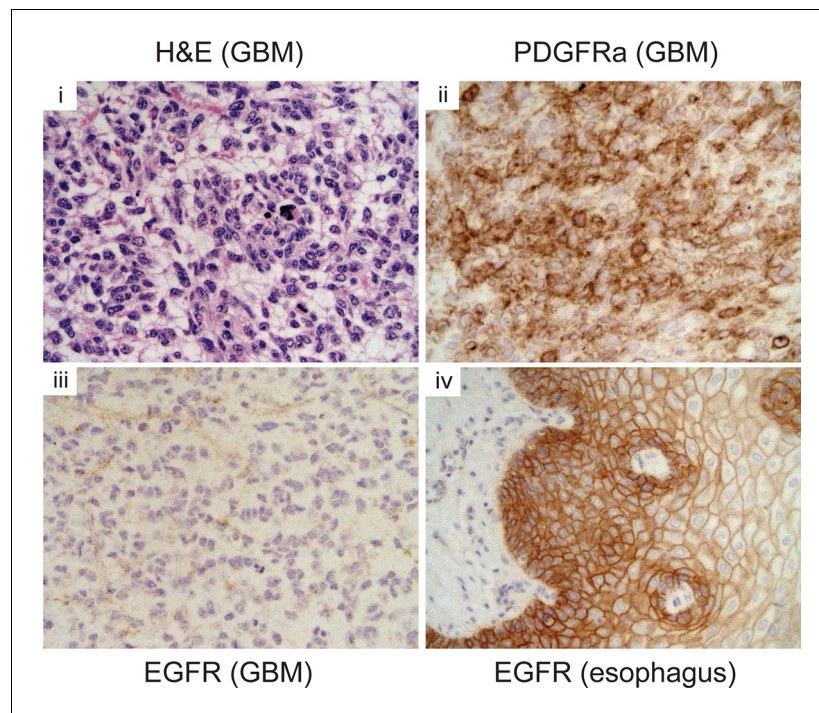


Figure 3—figure supplement 2. Pdgfra expression is elevated in $p53^{\Delta N}$ tumors, but Egfr is not. Immunohistochemistry of GBM sections showing elevated Pdgfra, but not Egfr, expression in a $p53^{\Delta N}$ tumor. Esophagus section is shown as positive control for Egfr staining. GBM, Glioblastoma multiforme
DOI: [10.7554/eLife.08711.018](https://doi.org/10.7554/eLife.08711.018)

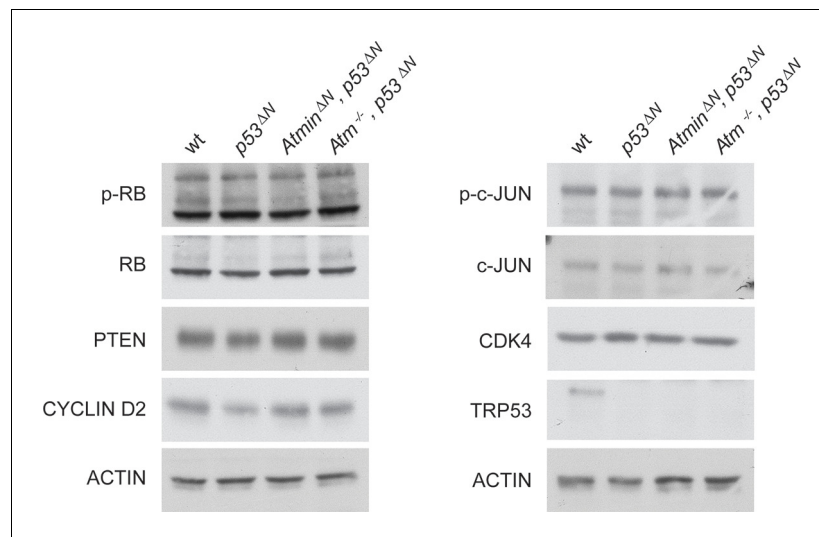


Figure 3—figure supplement 3. Some markers frequently altered in GBM are unaltered in p53^{ΔN} NSCs. Western blots of NSCs of the indicated genotypes showing levels of proteins commonly altered in glioma but unaffected by Atmin/Atm deletion. GBM, Glioblastoma multiforme; NSC, Neural stem cell

DOI: [10.7554/eLife.08711.019](https://doi.org/10.7554/eLife.08711.019)

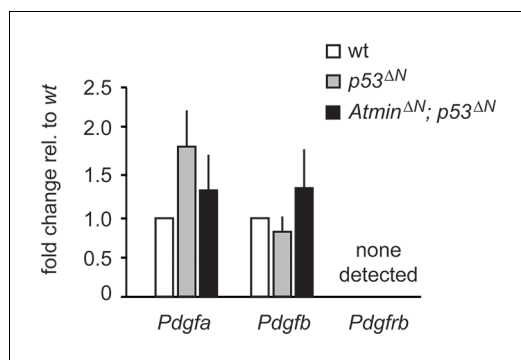


Figure 3—figure supplement 4. Pdgf ligand expression is not significantly altered in *p53^{ΔN}* NSCs. q-PCR showing similar expression levels of the Pdgfr ligands *Pdgfa* and *Pdgfb* in *p53^{ΔN}* and *Atmin^{ΔN}; p53^{ΔN}* cells. *Pdgfrb* was not detected. Error bars represent the SEM of at least three biological repeats. NSC, Neural stem cell.

DOI: [10.7554/eLife.08711.020](https://doi.org/10.7554/eLife.08711.020)

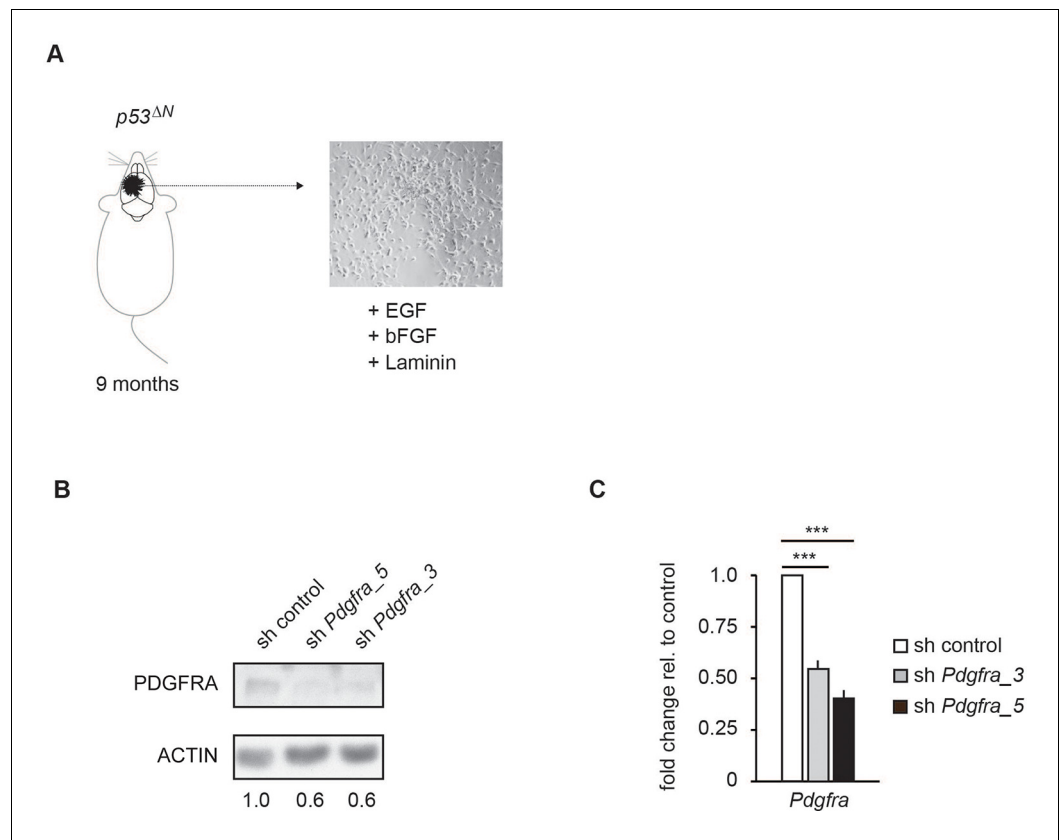


Figure 3—figure supplement 5. Two independent shRNAs cause *Pdgfra* knockdown. (A) Isolation and culture of *p53^{ΔN}* primary tumor cells from affected mice. (B–C) Western blot (B) and qPCR (C) showing knockdown of *Pdgfra* using two independent shRNA constructs. Error bars represent the SEM of at least two biological repeats. *** $p < 0.001$

DOI: [10.7554/eLife.08711.021](https://doi.org/10.7554/eLife.08711.021)

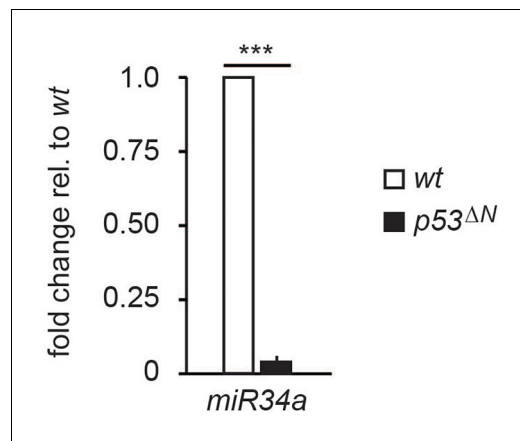


Figure 3—figure supplement 6. miR34a expression is reduced in p53 ΔN NSCs. Error bars represent the SEM of at least three biological repeats. *** p<0.001
DOI: [10.7554/eLife.08711.022](https://doi.org/10.7554/eLife.08711.022)

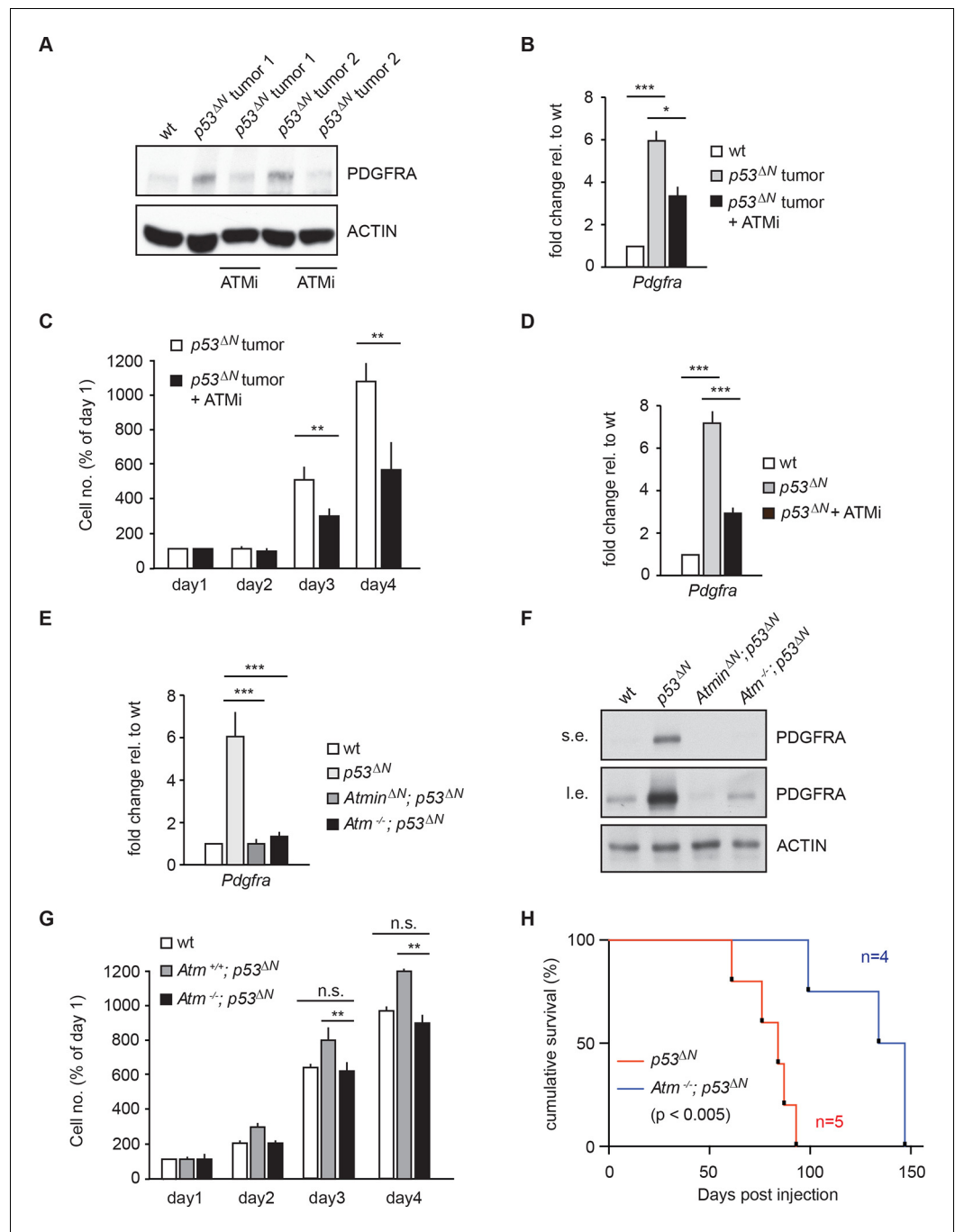


Figure 4. *Atm* inhibition reduces *Pdgfra* expression and reduces tumorigenic potential in murine $p53^{\Delta N}$ primary tumor cells and NSCs. (A–B) *Atm* inhibitor (ATMi) treatment reduces *Pdgfra* protein levels (A) and *Pdgfra* expression (B) in $p53^{\Delta N}$ primary tumor cells. (C) ATMi treatment reduces in vitro proliferation of $p53^{\Delta N}$ primary tumor cells. Error bars represent the SEM of two biological repeats. (D) ATMi reduces *Pdgfra* expression in $p53^{\Delta N}$ NSCs, assayed by qPCR. (E–F) *Pdgfra* expression (E) and *Pdgfra* protein levels (F) are reduced in $Atm^{-/-}; p53^{\Delta N}$ and $Atmin^{\Delta N}; p53^{\Delta N}$ compared with $p53^{\Delta N}$ NSCs. cDNA is normalized to *Actin* levels. Error bars represent the SEM of at least three biological repeats. s.e. and l.e. denote short and long exposures of the same blot, respectively. (G) Genetic loss of *Atm* reduces in vitro proliferation of $p53^{\Delta N}$ NSCs. Error bars represent the SEM of two biological repeats. (H) Kaplan-Meier curves indicating increased survival of NOD/SCID mice orthotopically transplanted with $Atm^{-/-}; p53^{\Delta N}$ NSCs compared with $p53^{\Delta N}$ NSCs. n.s., not significant; * $p < 0.05$, ** $p < 0.01$, *** $p < 0.001$. NSC, Neural stem cell.

DOI: 10.7554/eLife.08711.023

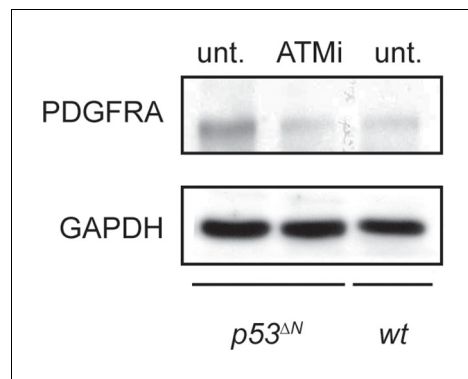


Figure 4—figure supplement 1. ATM inhibitor (ATMi) treatment reduces Pdgfra protein levels in $p53^{\Delta N}$ NSCs. NSCs, Neural stem cells.
DOI: [10.7554/eLife.08711.024](https://doi.org/10.7554/eLife.08711.024)

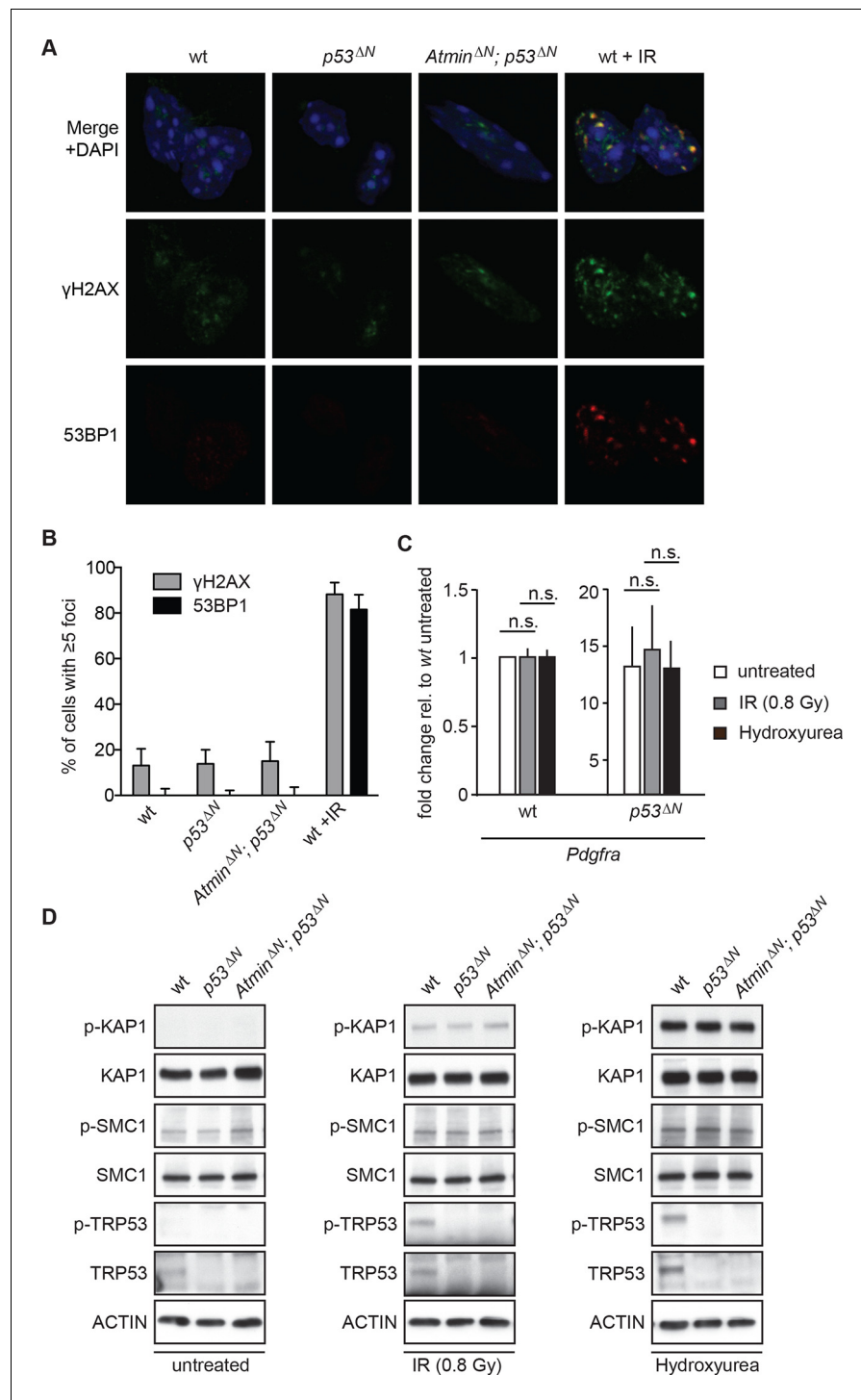


Figure 5. Atm signaling in response to DNA damaging agents is remarkably unaffected in *p53^{ΔN}* and *Atmin^{ΔN}*; *p53^{ΔN}* cells and DNA damaging treatments do not affect *Pdgfra* expression. (A) *p53^{ΔN}* and *Atmin^{ΔN}*; *p53^{ΔN}* NSCs do not show elevated γ h2ax and 53bp1 foci in untreated conditions, suggesting low endogenous damage. Cells treated with 5Gy IR (wt +IR) are shown as a positive control. (B) Quantification of γ h2ax and 53bp1 foci in (A). Error bars indicate 95% confidence intervals. (C) qPCR of *Pdgfra* in wt and *p53^{ΔN}* NSCs in untreated conditions and after DNA damage-inducing stimuli. cDNA is normalized to *Actin* levels. Error bars represent SEM of three biological repeats. (D) Western blots depicting Atm substrate phosphorylation after the indicated stimuli in NSCs of different genotypes.

DOI: 10.7554/eLife.08711.025

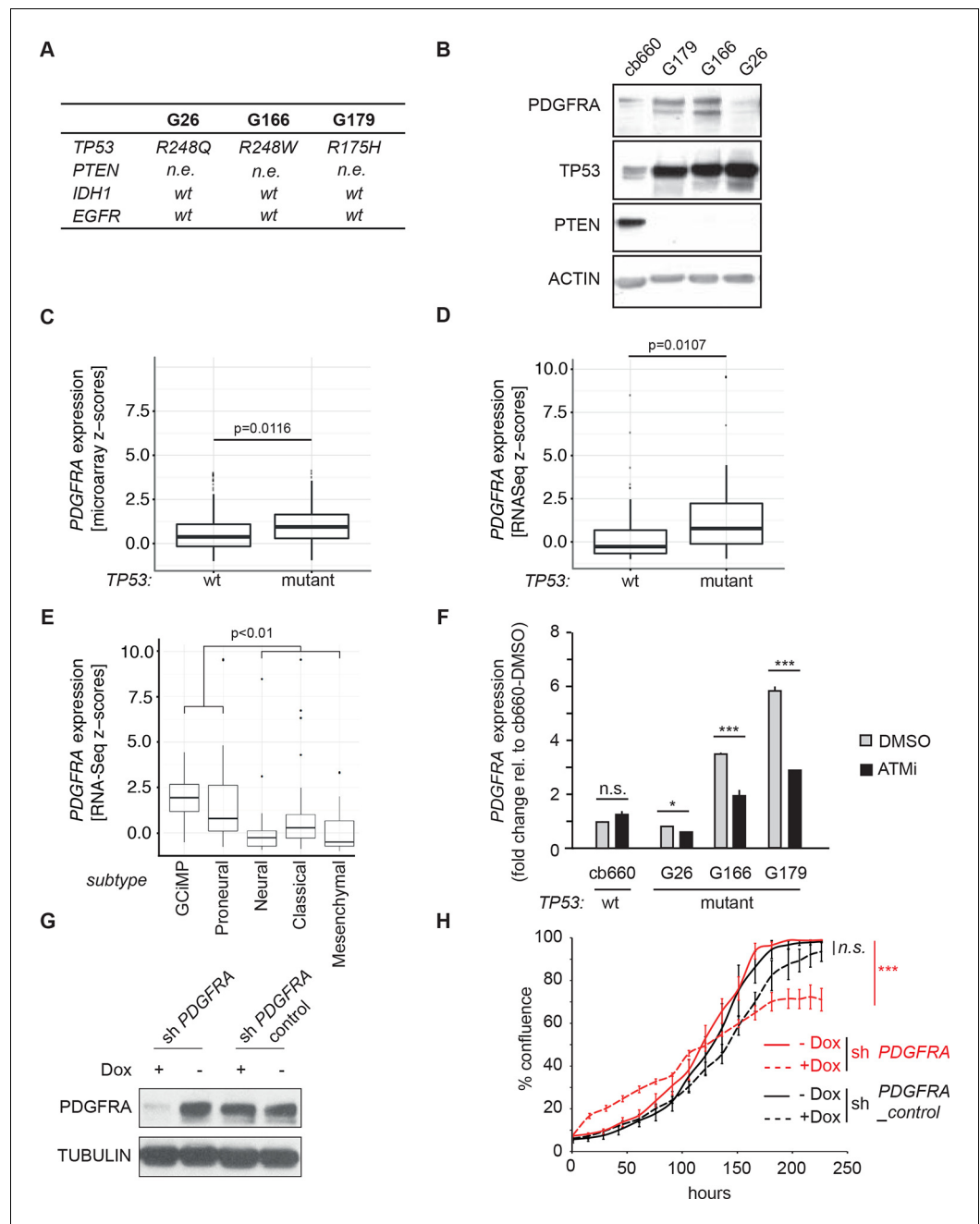


Figure 6. ATM inhibitor treatment reduces elevated PDGFRA expression and decreases proliferation in human GBM tumor cells. (A) Mutational status of *TP53*, *PTEN*, *IDH1*, and *EGFR* in the indicated glioma neural stem cell (GNSC) lines. n.e., not expressed. wt, wild type. (B) Western blot depicting PDGFRA, TP53, PTEN, and ACTIN expression in three GNSC lines (G26, G166, and G179) and cb660 control cells. (C,D) Box plots showing PDGFRA expression in TP53-wt and TP53-mutant TCGA human glioblastoma datasets, measured by microarray (n=153) (C) or RNA-Seq (n=500). (D) Data from 518 patient samples in total with an overlap of 135 patients. (E) Box plots showing PDGFRA expression z-scores in TCGA human glioblastoma subtypes, measured by RNA-Seq (n=150). p-Values in (C–E) calculated using Wilcoxon’s test. (F) qRT-PCR showing decreased PDGFRA expression in TP53-mutant GNSC lines after ATM inhibitor (ATMi) treatment. cDNA is normalized to GAPDH levels. Error bars represent the STDEV of two biological repeats. (G) Western blot showing knockdown of PDGFRA using a doxycycline (Dox)-inducible shRNA construct. (H) PDGFRA knockdown using doxycycline (Dox)-inducible shRNA reduces proliferation of TP53-mutant G179 GNSCs. Cell confluence measured by IncuCyte timelapse microscopy. Error bars represent the SEM of three biological repeats. * p<0.05, *** p<0.001, n.s., not significant. Figure 6 continued on next page

Figure 6 continued

DOI: [10.7554/eLife.08711.026](https://doi.org/10.7554/eLife.08711.026)

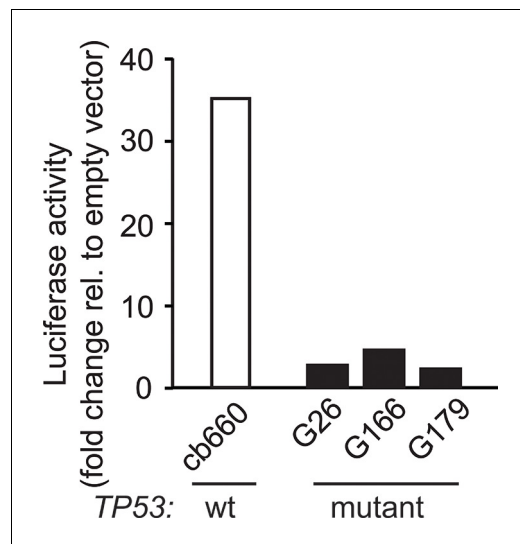


Figure 6—figure supplement 1. Luciferase reporter assay for TP53 activity using the p53-550RE construct in human GNSC (G26, G166, G179) and control NSC (cb660) lines. NSC, Neural stem cell.

[DOI: 10.7554/eLife.08711.027](https://doi.org/10.7554/eLife.08711.027)

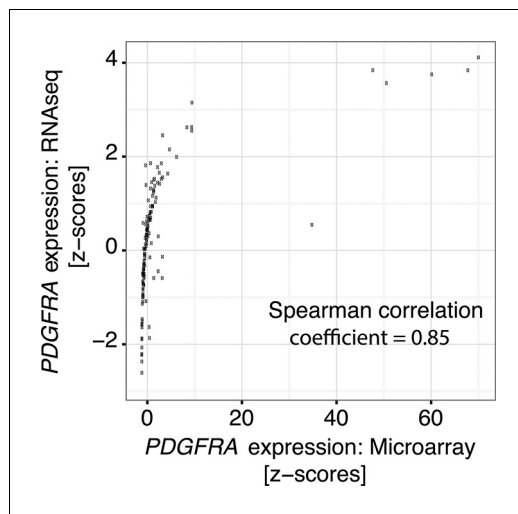


Figure 6—figure supplement 2. Correlation of *PDGFRA* expression levels in TCGA glioblastoma samples represented in both microarray and RNAseq datasets.

DOI: [10.7554/eLife.08711.028](https://doi.org/10.7554/eLife.08711.028)

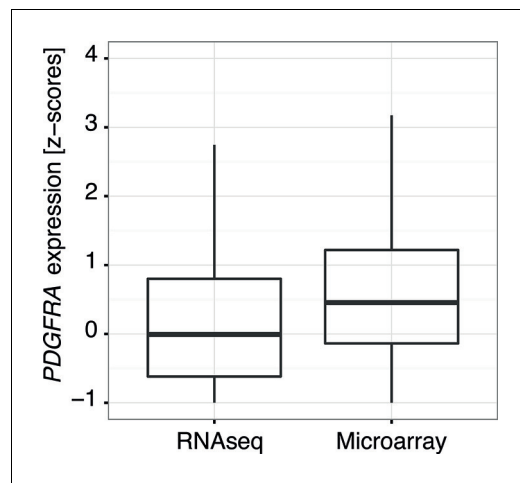


Figure 6—figure supplement 3. Comparison of the distribution of *PDGFRA* expression levels in human glioblastoma samples measured by RNASeq and by microarray. Data from TCGA.
DOI: [10.7554/eLife.08711.029](https://doi.org/10.7554/eLife.08711.029)

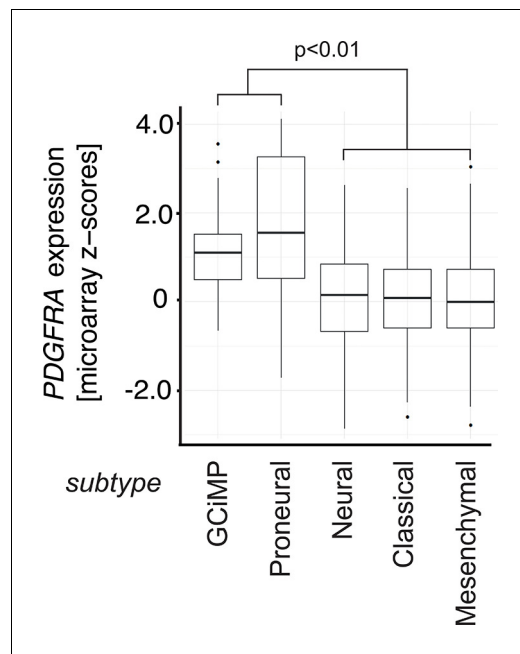


Figure 6—figure supplement 4. Box plots showing *PDGFRA* expression z-scores in TCGA human glioblastoma subtypes measured by microarray (n=487). p-Value is calculated using Wilcoxon's test, combining GCiMP and Proneural versus Neural, Classical, and Mesenchymal.

DOI: [10.7554/eLife.08711.030](https://doi.org/10.7554/eLife.08711.030)

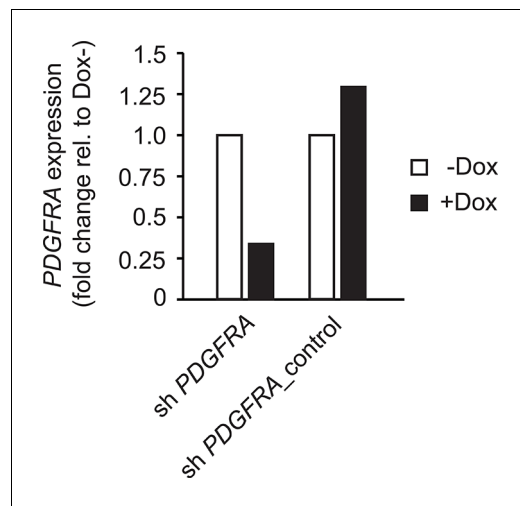


Figure 6—figure supplement 5. Control for **Figure 6G and H** showing efficient knockdown of *PDGFRA* after doxycycline administration. q-PCR showing knockdown of *PDGFRA* in GNSCs using a doxycycline (Dox)-inducible shRNA construct. DOI: [10.7554/eLife.08711.031](https://doi.org/10.7554/eLife.08711.031)

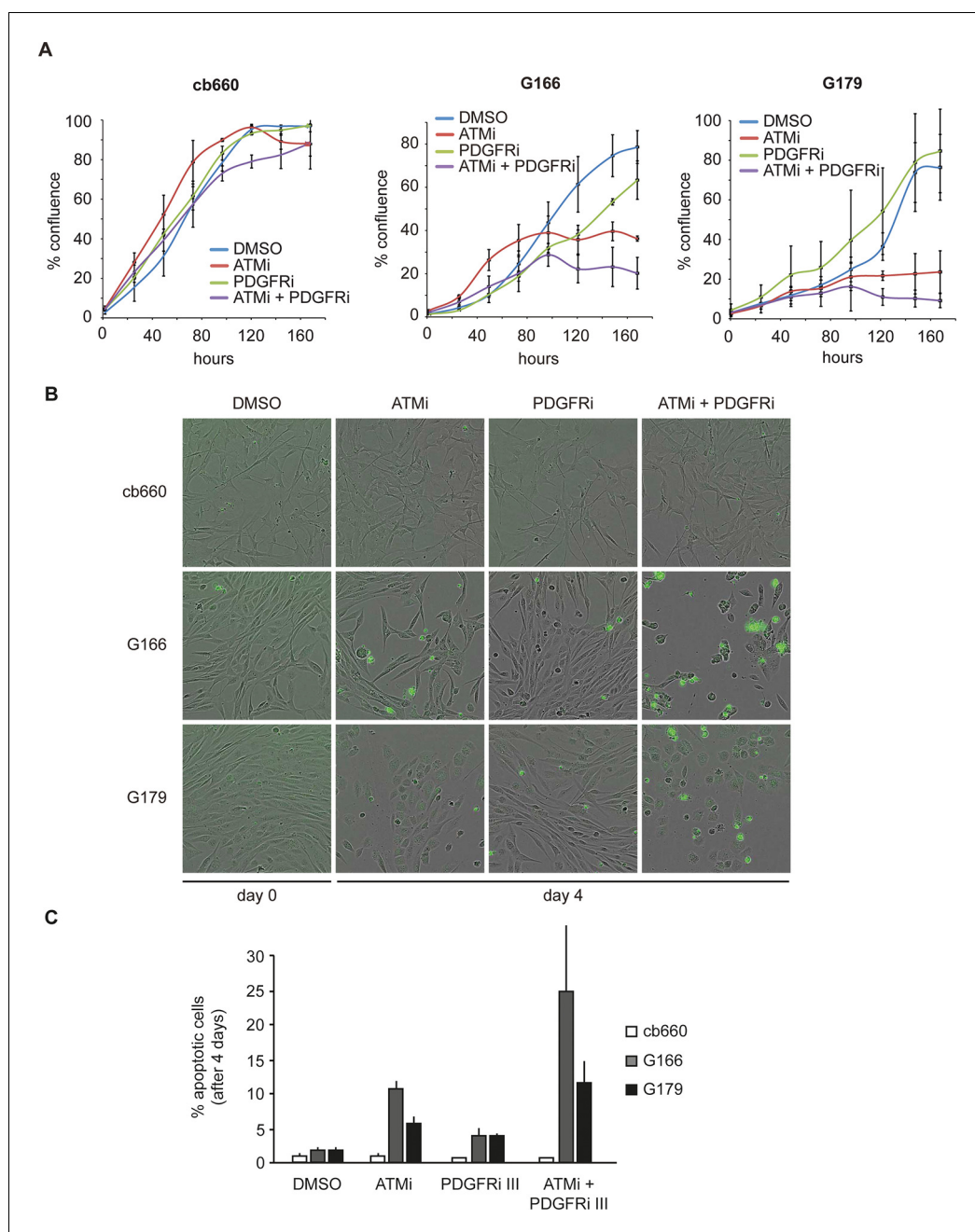


Figure 7. Combinatorial treatment with both ATM and PDGFR inhibitors induces apoptosis of human glioma stem cells. **(A)** Growth curves showing the proliferation of wild-type control human neural stem cells (cb660) and two independent cell lines isolated from TP53-deficient human gliomas (G166 & G179) over 7 days in the presence of vehicle control (DMSO), ATM inhibitor (ATMi), PDGFR inhibitor (PDGFRi), or both inhibitors. Error bars depict STDEV from two biological repeats. **(B)** Representative bright-field/fluorescent images of the same cell types treated as above after 4 days. Cells undergoing apoptosis are labeled by emitting GFP. **(C)** Quantification of apoptotic cells after the treatments indicated above, represented as % apoptotic cells from total live cells. Error bars depict STDEV from three biological repeats. After four days, it became impossible to quantify apoptotic GNSCs receiving the combination treatment, since they detached completely from the culture plate. These percentages thus represent an underestimate of the total extent of G166 and G179 cell death with ATMi + PDGFRi.

DOI: [10.7554/eLife.08711.032](https://doi.org/10.7554/eLife.08711.032)

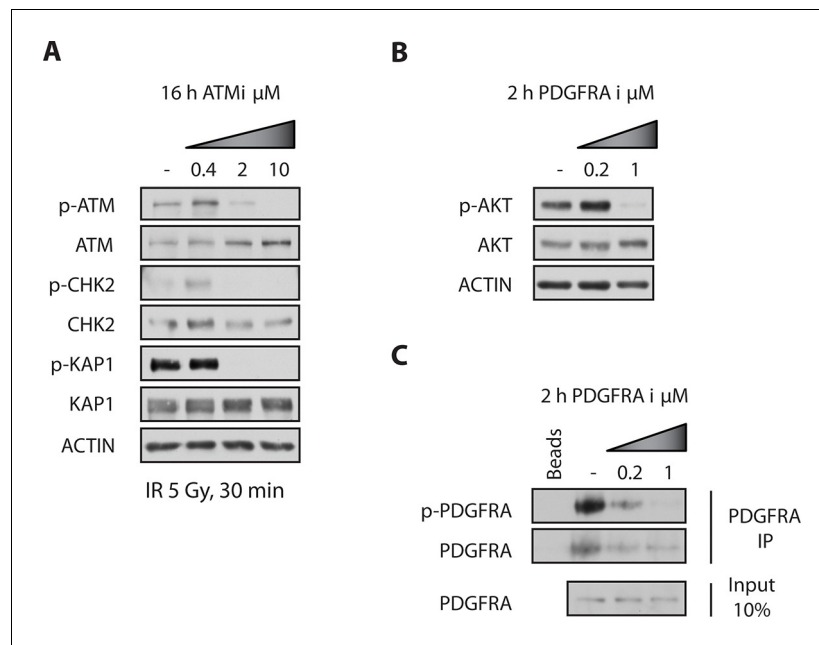


Figure 7—figure supplement 1. ATM and PDGFR inhibitors were used at minimally required concentration to achieve pathway inhibition. **(A)** G179 cells were treated with DMSO or 400 nM, 2 μM or 10 μM of ATMi for 16 hrs, then subjected to 5Gy of ionizing irradiation, harvested 30 min later and analyzed by Western blotting. Pre-treatment of cells with the ATMi at 10 μM clearly prevented IR-induced ATM auto-phosphorylation at Serine 1981 and phosphorylation of its downstream substrates: KAP1 and CHK2, at Serine 824 and Threonine 68, respectively. **(B)** G179 cells were treated with DMSO, 200 nM or 1 μM of PDGFRA inhibitor III for 2 hrs, harvested and analyzed by Western blotting. 1 μM inhibitor prevented the phosphorylation of AKT (downstream substrate of PDGFRA) at Serine 473. **(C)** P-PDGFR levels were below detection, therefore total PDGFRA was immunoprecipitated from cell lysates prior to Western blotting. Treatment of cells with the PDGFRA inhibitor III at 1 μM clearly reduced phosphorylation of PDGFRA at Tyrosine 754.

DOI: [10.7554/eLife.08711.033](https://doi.org/10.7554/eLife.08711.033)

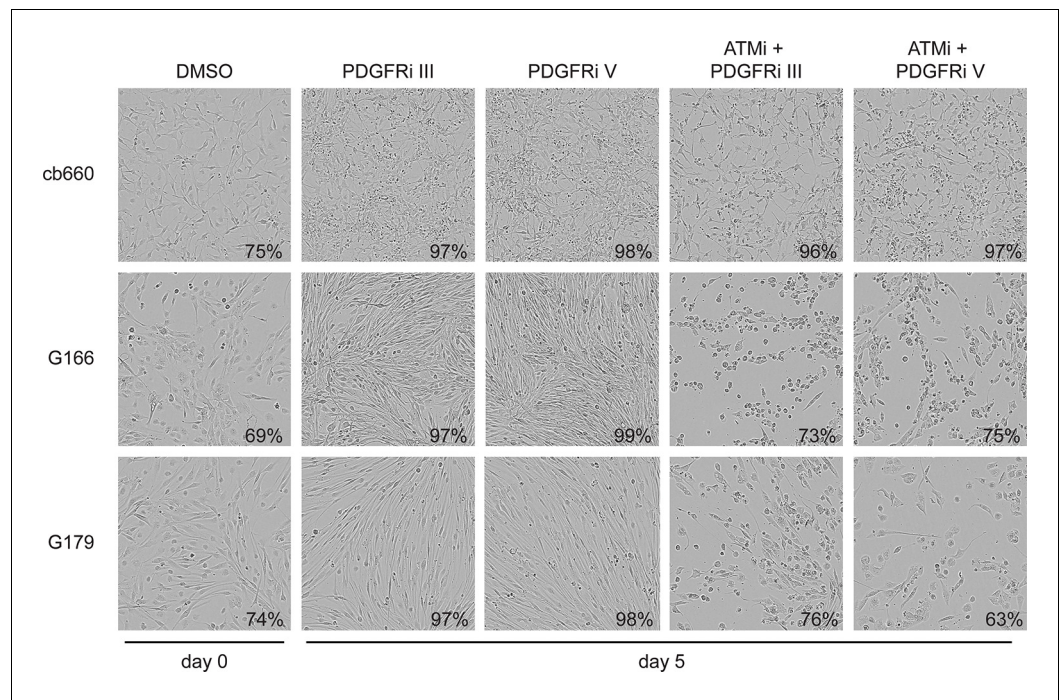


Figure 7—figure supplement 2. Bright-field images of timelapse microscopy using cells seeded at high confluency. Representative bright-field images of cb660, G166, and G179 GNSC lines seeded at high confluency and treated over 7 days with vehicle control (DMSO), ATM inhibitor (ATMi), PDGFR inhibitors III or V, or both ATM and PDGFR inhibitors. Values indicate % confluency at the indicated point in the time course as measured using IncuCyte software.

DOI: [10.7554/eLife.08711.034](https://doi.org/10.7554/eLife.08711.034)

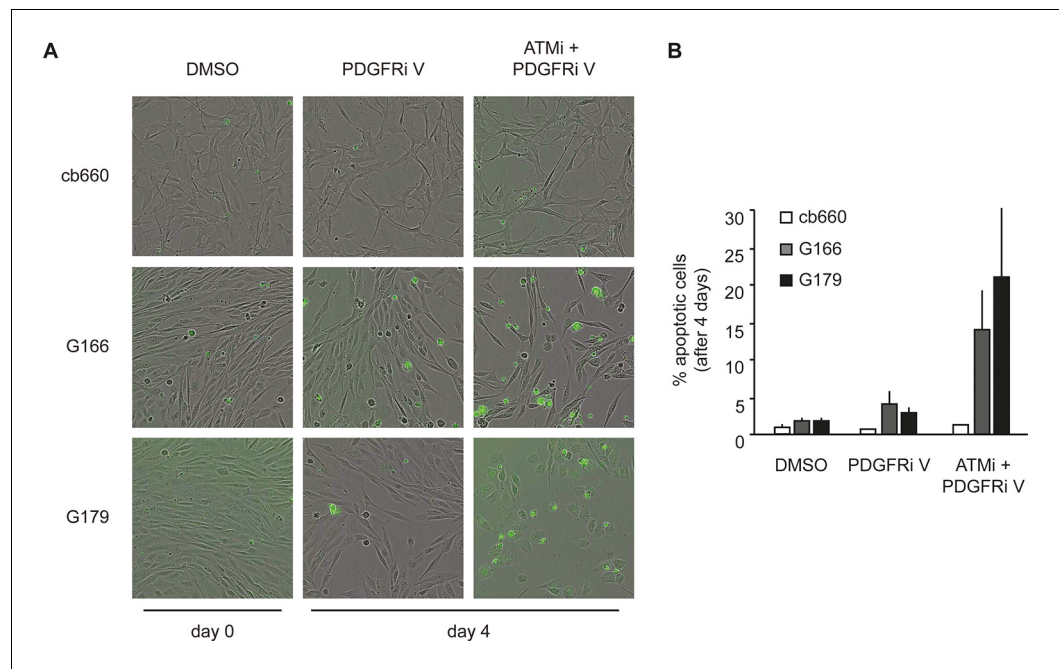


Figure 7—figure supplement 3. Apoptosis quantification of a second PDGFR inhibitor. (A) Representative bright-field/fluorescent images of the same cell types treated over 4 days with vehicle control (DMSO), PDGFR inhibitor V (PDGFRi V), or ATM inhibitor in combination with PDGFR inhibitor V (ATMi + PDGFRi V). Cells undergoing apoptosis are labelled by emitting GFP. (B) Quantification of apoptotic cells four days after the treatments indicated above, represented as % apoptotic cells from total live cells. After four days, it became impossible to quantify apoptotic GNSCs receiving the combination treatment, since they detached completely from the culture plate. These percentages thus represent a large underestimate of the extent of G166 and G179 cell death with ATMi + PDGFRi V.

DOI: [10.7554/eLife.08711.035](https://doi.org/10.7554/eLife.08711.035)